Electronic Supplementary Material (ESI) for Journal of Materials Chemistry A.

Electronic Supplementary Information

High and energy-efficient reversible SO_2 uptake by a robust Sc(III)-based MOF

J. Antonio Zárate,†[a,b] Elí Sánchez-González,†[a] Daryl R. Williams,[c] Eduardo González-Zamora,[d] Vladimir Martis,[e] Jorge Balmaseda,[f] Ana Martínez,[d,f] Guillaume Maurin*[,b] and Ilich A. Ibarra*[,a]

a. Laboratorio de Fisicoquímica y Reactividad de Superficies (LaFReS), Instituto de Investigaciones en Materiales, Universidad Nacional Autónoma de México, Circuito Exterior s/n, CU, Del. Coyoacán, 04510, Ciudad de México, Mexico.

b. Institut Charles Gerhardt Montpellier, UMR-5253, Université de Montpellier, CNRS, ENSCM, Place E. Bataillon, 34095 Montpellier cedex 05, France.

c. Surfaces and Particle Engineering Laboratory (SPEL), Department of Chemical Engineering, Imperial College London, South Kensington Campus, London SW7 2AZ, U.K.

d. Departamento de Química, Universidad Autónoma Metropolitana-Iztapalapa, San Rafael Atlixco 186, Col. Vicentina, Iztapalapa, C. P. 09340, Ciudad de México, Mexico.

e. Surface Measurement Systems, Unit 5, Wharfside, Rosemont Road, London HA0 4PE, U.K.

f. Instituto de Investigaciones en Materiales, Universidad Nacional Autónoma de México, Circuito Exterior s/n, CU, Del. Coyoacán, 04510, Ciudad de México, Mexico.

* Corresponding Authors

E-mail: argel@unam.mx and guillaume.maurin1@umontpellier.fr

† These authors contributed equally to this work.

1. Crystal Structure of MFM-300(Sc)

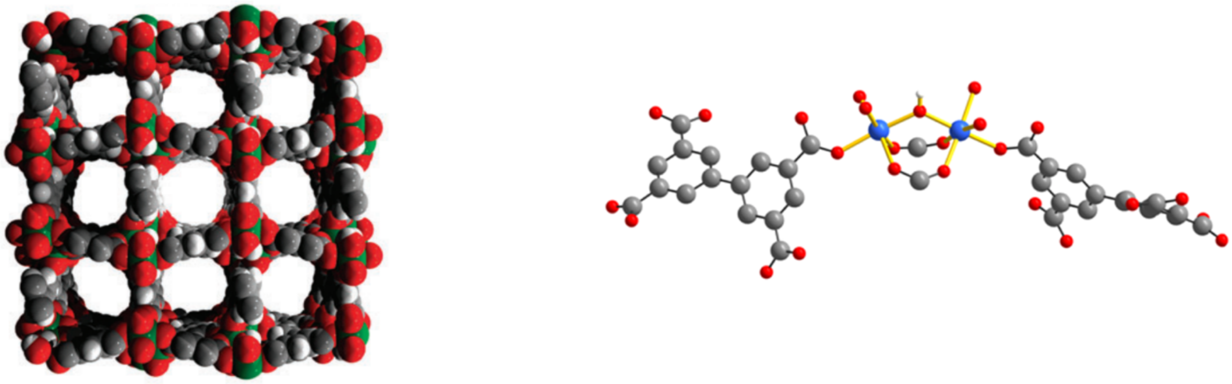

Fig. S1. (left) space-filling view of the structure of MFM-300(Sc) along the *b*-axis showing 8.1 Å channels (Reproduced from Ref. 1 with permission from The Royal Society of Chemistry); and (right) view of the coordination at Sc(III) in MFM-300(Sc), showing $[BPTC]^{4-}$ and the μ_2-OH group (Reproduced from Ref. 9 with permission from The American Chemical Society).

2. Experimental Details

Chemicals

Scandium triflate ($Sc(SO_3CF_3)_3 \cdot xH_2O$), biphenyl-3,3′,5,5′-tetracarboxylic acid (H_4BPTC), *N*,*N*-dimethylformamide (DMF), and tetrahydrofuran (THF) were purchased from Sigma-Aldrich or Fisher Scientific and used as received.

Synthesis of MFM-300(Sc)

MFM-300(Sc) ($[Sc_2(OH)_2(BPTC)]$) was synthesised according to a procedure previously reported:[1] Scandium triflate (0.030g, 0.061 mmol) and H_4BPTC (0.010 g, 0.030 mmol) were mixed in THF (4.0 ml), DMF (3.0 ml), water (1.0 ml) and HCl (36.5 %, 2 drops). The resultant slurry mixture was stirred until complete dissolution occurred. The solution was then placed in a pressure tube and heated in an oil bath to 75 °C for 72 h. The tube was cooled down to room temperature at a rate of 0.1 °C/min, and the colourless crystalline product was separated by filtration, washed with DMF (5.00 ml) and dried in air. Yield: 66.4 % (based on ligand).

Measurements

Powder X-ray diffraction (PXRD) data were collected under ambient conditions on a Bruker AXD D8 Advance diffractometer operated at 160 W (40 kV, 40 mA) for Cu Kα_1 (λ= 1.5406 Å). Thermal gravimetric analysis (TGA) was performed under N_2 at a scan rate of 2 °C/min using a TA Instruments Q500HR analyser. N_2 adsorption was carried out in a conventional volumetric technique by a Micromeritics ASAP 2020 sorption meter. The surface area was calculated using the BET method based on adsorption data in the partial pressure (P/P_0) range 0.01 to 0.04.

3. PXRD of the as-synthesised MFM-300(Sc)

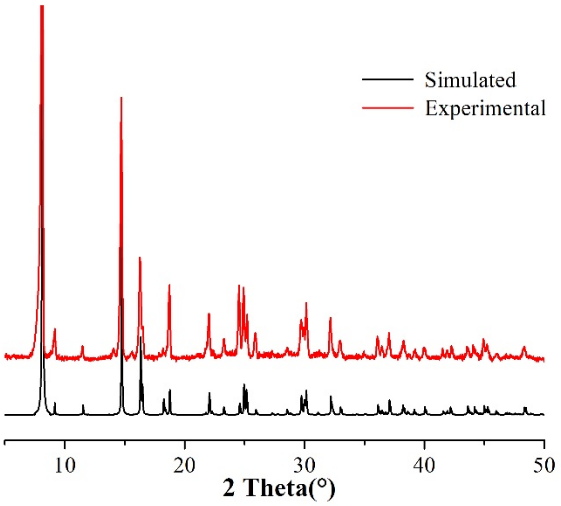

Fig. S2. Simulated PXRD pattern for MFM-300(Sc), (black) and the as-synthesised (experimental) pattern (red) for MFM-300(Sc).

4. TGA of the as-synthesised MFM-300(Sc)

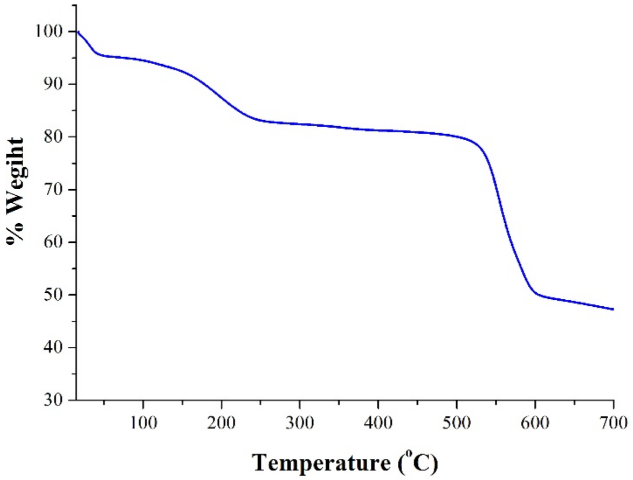

Fig. S3. TGA of the as-synthesised MFM-300(Sc).

5. N_2 adsorption-desorption for activated MFM-300(Sc)

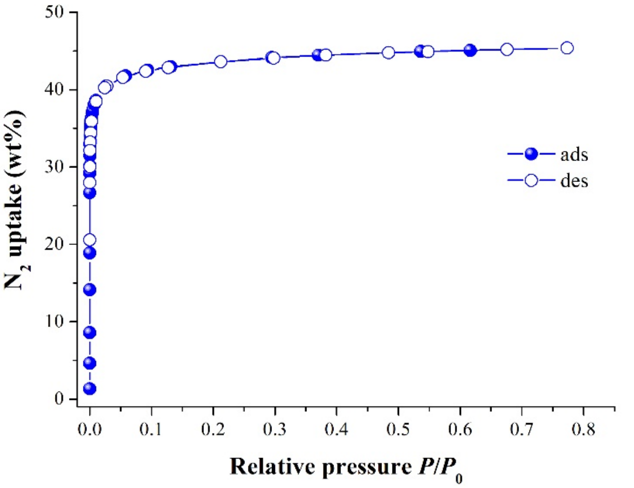

Fig. S4. N_2 adsorption-desorption isotherm at 77 K for activated (453 K and 1.7×10^{-3} Torr for 100 min) for MFM-300(Sc). The BET surface area estimated for MFM-300(Sc) was of approximately 1360 m^2 g^{-1}.

6. PXRD and N_2 sorption experiments of MFM-300(Sc) after SO_2 adsorption-desorption

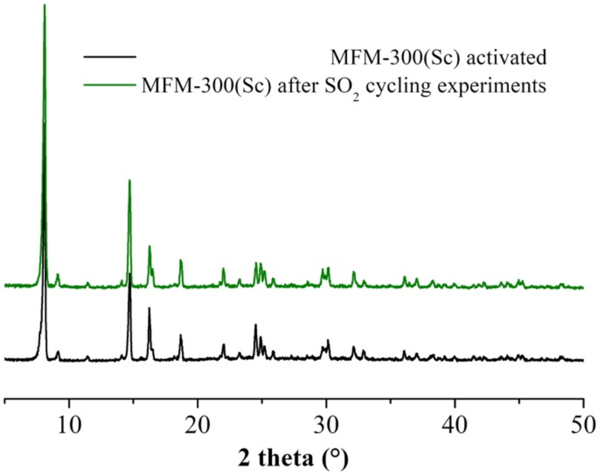

Fig. S5. Activated (453 K and 1.7×10^{-6} Torr for 100 min) PXRD pattern for MFM-300(Sc) (black) and the pattern of MFM-300(Sc) after ten cycles of SO_2 (green).

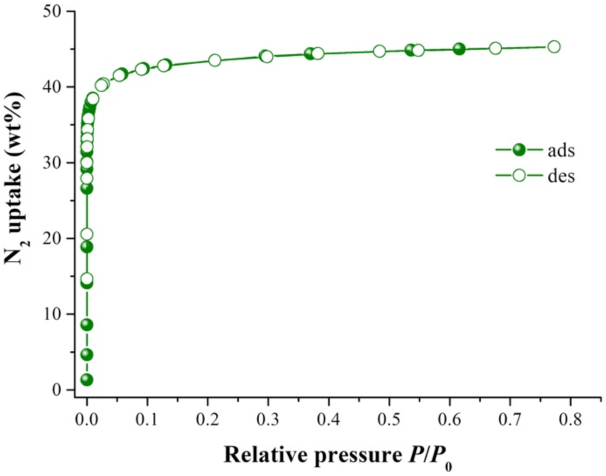

Fig. S6. N_2 adsorption-desorption isotherm at 77 K for MFM-300(Sc) after ten cycles (adsorption-desorption) of SO_2 (cycled sample was activated at 453 K and 1.7×10^{-3} Torr for 100 min). The BET surface area estimated for cycled MFM-300(Sc) was of approximately 1348 m^2 g^{-1}.

7. Enthalpy of adsorption for SO_2

The enthalpy of adsorption was estimated using the isosteric method, with two approaches.[2,3] The fitting of the adsorption isotherms at two different temperatures, 298 and 303 K with the Clausius-Clapeyron equation allowed us to estimate the isosteric heat of adsorption at a zero-coverage. The so-obtained value (-36.2 kJ mol^{-1}) is above the enthalpy of vaporization for SO_2 (-22.92 kJ mol^{-1}) at 298 K.

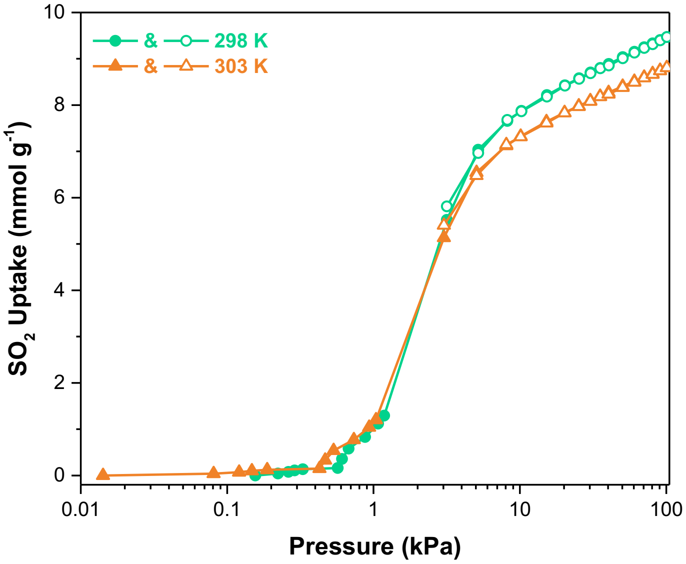

Fig.S7. SO_2 adsorption isotherms of MFM-300(Sc) at 298 and 303 K.

In this approach a virial-type equation (Eq. 1) was used to fit the low coverage region of two adsorption isotherms:

Eq. 1. $ln\left(\frac{n}{p}\right) = A_0 + A_1 n + A_2 n^2 + \cdots$

where p is the pressure, n is the amount adsorbed and A_0, A_1, ... are the virial coefficients (A_2 and higher terms can be ignored at lower coverage values). A plot of $ln(n/p)$ versus n should give a straight line at low surface coverage (Fig. S8).

Using the Clausius-Clapeyron equation (Eq. 2) for a fixed surface coverage (n), the Eq. 3 is obtained. By the substitution of p in Eq. 3 with Eq. 1, results an expression of the enthalpy of adsorption (Eq. 4). From the linear fittings, the virial coefficients are used to estimate the enthalpy of adsorption.

Eq. 2. $\left(\frac{\partial ln(p)}{\partial T}\right)_n = -\frac{\Delta H_{ads}}{RT^2}$

Eq. 3. $ln\left(\frac{p_1}{p_2}\right) = -\frac{\Delta H_{ads}}{R}\left(\frac{1}{T_2} - \frac{1}{T_1}\right)$

Eq. 4. $\Delta H_{ads} = -R\left[\left(A_0^{T_2} - A_0^{T_1}\right) + \left(A_1^{T_2} - A_1^{T_1}\right)n\right]\left(\frac{T_1T_2}{T_1-T_2}\right)$

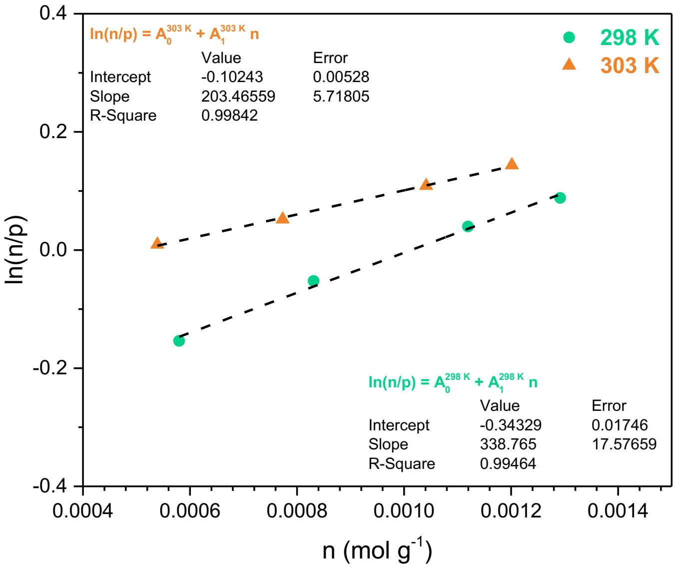

Fig. S8. Virial fitting plots for the adsorption isotherms of SO_2 for MFM-300(Sc).

8. Ideal Adsorbed Solution Theory (IAST)

The predictions of the co-adsorption of SO_2:CO_2 mixtures in MFM-300(Sc) were carried out assuming valid the *Ideal Adsorbed Solution Theory (IAST)* hypotheses[4] and using Python package pyIAST.[5] Experimental CO_2 isotherm was measured up to 20 bar in order to obtain comparable distributed pressure data to that of SO_2 (1 bar) and be able to make reliable IAST calculations. Langmuir analytical isotherm was fitted to CO_2 experimental isotherm with not significant root mean square error (Fig. S11). None of the available analytical models in pyIAST fitted the experimental SO_2 isotherm. Thus, the SO_2 adsorption data was linearly interpolated (Fig. S12) and distributed pressures were calculated by numerical quadrature implemented in pyIAST. In any extrapolation beyond the highest experimental SO_2 equilibrium pressure it was assumed that the saturation loading is equal to the highest uptake in the data. Therefore, the adsorption selectivity was calculated as:[4,6]

$$S_{\mathrm{SO_2/CO_2}} = \frac{x_{\mathrm{SO_2}} y_{\mathrm{CO_2}}}{x_{\mathrm{CO_2}} y_{\mathrm{SO_2}}}$$

where, x_i and y_i are the mole fraction of the component i = SO_2, CO_2 in adsorbed and gas phase respectively.

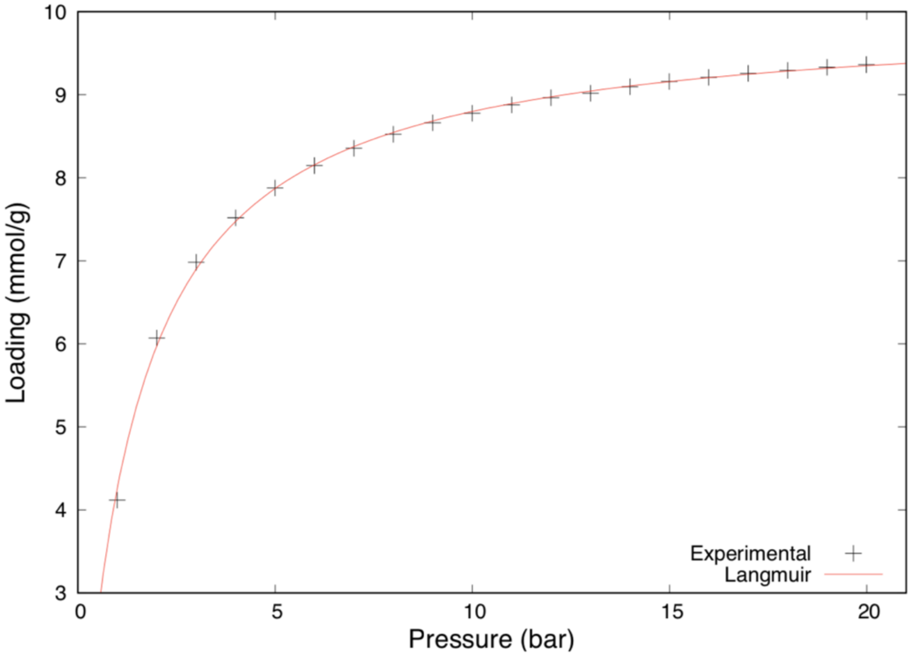

Fig. S9. Experimental CO_2 adsorption isotherm at 25°C (black crosses) and Langmuir analytical isotherm fitted to experimental data (continuous red line).

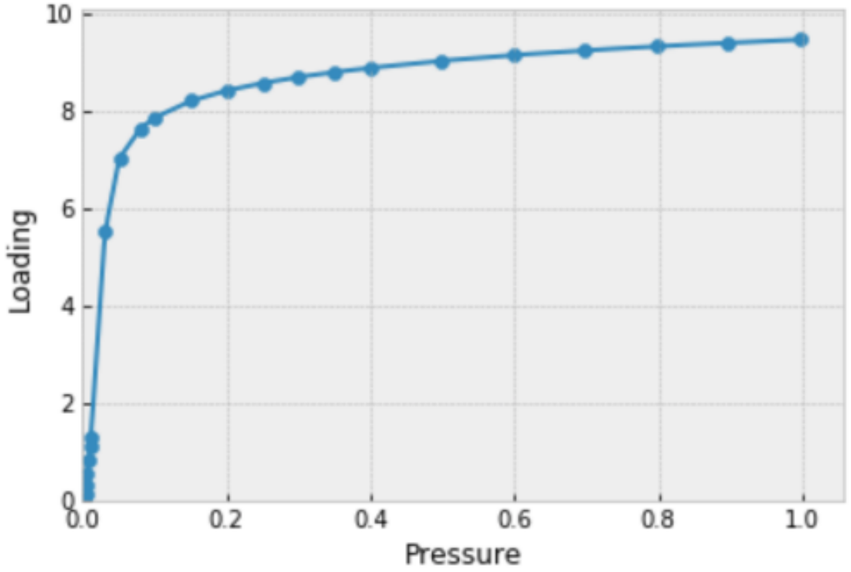

Fig. S10. Experimental SO_2 adsorption isotherm at 298 K (full circles) and the interpolation model fit (continuous line). Loading in mmol/g and Pressure in bar.

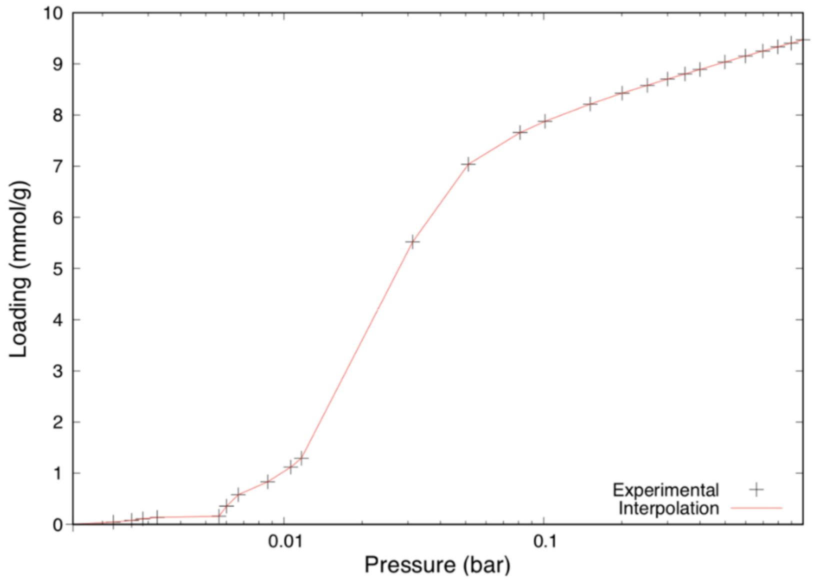

Fig. S11. Experimental SO_2 adsorption isotherm at 25 ˚C (black crosses) and the interpolation model fit (continuous red line). A semi-log scale was used to show the experimental details at low pressures.

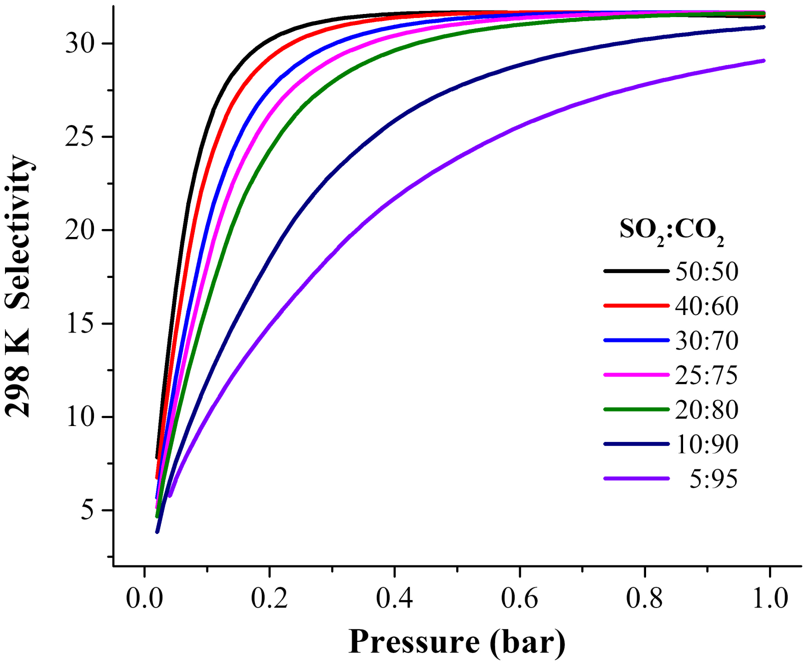

Fig. S12. IAST selectivity of SO_2/CO_2 mixtures in MFM-300(Sc) to a pressure of 1 bar at 298 K.

9. Monte Carlo Simulations

Microscopic models for MFM-300(Sc), SO_2 and CO_2 and interatomic potentials

Initial atomic coordinates for MFM-300(Sc) were taken from a previously reported study[1]. The Lennard-Jones (LJ) parameters for the organic and inorganic parts of MFM-300(Sc) were taken from DREIDING[11] force field and the UFF[12] force field respectively. The partial atomic charges for each framework atom of MFM-300(Sc) were extracted from periodic Density Functional Theory (DFT) calculations using the ESP[13] method as implemented in Dmol[3] and the PBE[14] functional and the DNP[15] basis set. The SO_2 molecule was represented by the model reported by Ketko *et. al.*[16]. This corresponds to a rigid model where both three charged LJ sites are centered in the atomic positions, with a S-O bond of 1.432 Å and a O-S-O bond angle of 119.3°. On the other hand, the CO_2 was represented by the TraPPE model[17]. This model has three charged LJ sites centered in the atomic positions, with a C-O bond of 1.160 Å and a O-C-O bond angle of 180.0°. The H_2O molecule was treated by the TIP4P/2005 model[18], this is a four-site model, with a single LJ site centered in the O-atom position and three charged sites, two centered in the H-atoms positions and one called M located at a distance of 0.1546 Å of the hydroxyl-O atom in the molecule bisector axis, having an O–H bond length of 0.9572 Å. The MFM-300(SC)-SO_2/CO_2 interactions were described using a 12-6 LJ potential and a coulombic contribution. Using a general approach adopted in previous studies[19], the H atom from the μ-OH group and the Sc atoms interacts with the guest molecules only through electrostatic interactions. LJ crossed parameters between the MOF material and the guest molecules were calculated with the Lorentz-Berthelot mixing rules. A cut off distance of 12 Å was used for the LJ contributions, while the long-range electrostatic interactions were handled with the Ewald summation technique[20].

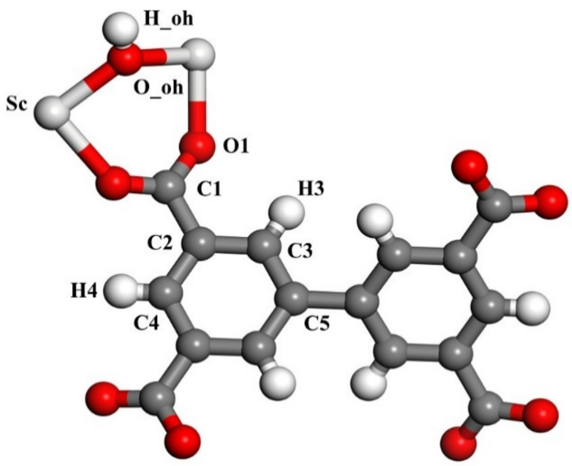

Fig. S13. Labels of the atoms for the organic and inorganic parts of MFM-300(Sc).

Table S1. LJ potential parameters and charges for the atoms of the MFM-300 (Sc).

Atom Type	ε (K)	σ (Å)	Charge
Sc	0.000	2.9357	1.5350
C1	47.856	3.4732	0.4820
C2	47.856	3.4732	0.0290
C3	47.856	3.4732	-0.1850
C4	47.856	3.4732	-0.1860
C5	47.856	3.4732	0.0820
H3	7.6489	2.8466	0.1380
H4	7.6489	2.8466	0.1420
H_oh	0	2.5713	0.4820
O1	48.158	3.0333	-0.4560
O_oh	92.123	3.1183	-1.1590

Table S3. LJ potential parameters and charges for the atoms of the SO_2, CO_2 and H_2O molecules.

Atom Type	ε (K)	σ (Å)	Charge
S_so2	73.800	3.3900	0.5900
O_so2	79.000	3.0500	-0.2950
C_co2	28.129	3.3900	0.6512
O_co2	80.507	3.033	-0.3256
O_h2o	93.200	3.1589	0
H_h2o	0	0	0.5564
M_h2o	0	0	-1.1128

Details of Monte Carlo Simulations

A simulation box was made of 4 units cell (2×2×1) for the computational simulations, by fixing all atoms of the framework in their initial positions. All MC simulations were performed using the simulation code CADSS (Complex Adsorption and Diffusion Simulation Suite),[21] with the consideration of 2.10^7 cycles in each of the simulations.

MC simulations in the μVT ensemble were carried out at 298 K to predict the adsorption behaviour of SO_2 as single component, in the presence of water (relative humidity of 10% and 20% corresponding to 2.1 and 4.5 H_2O molecules per unit cell based on the experimental adsorption isotherm) and mixture with CO_2 (gas molar composition SO_2/CO_2: 20/80) in the range of 0.01 to 1 bar. The fugacity used for each of the simulations was calculated using the Peg-Robinson equation.

Complementary MC simulations were carried out in the NVT ensemble to explore the preferential adsorption sites of SO_2 and CO_2 as a single component and as mixture at low, intermediate and high loading. These studies involved the analysis of the radial distribution functions (RDFs) plotted between different MOF/guest atoms pairs calculated for hundreds of MC configurations. The adsorption enthalpies at low coverage were also calculated using the revised Widom test particle insertion[22].

Simulated adsorption isotherms for SO_2 in dry and humidity conditions

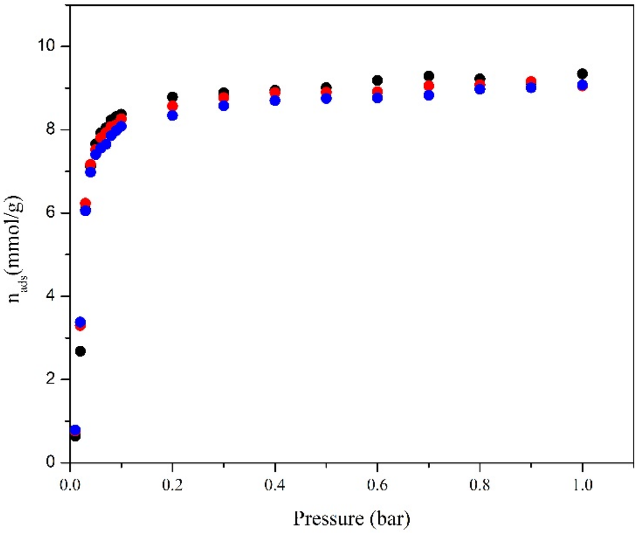

Fig. S14. GCMC simulated SO_2 adsorption isotherm for fully dehydrated MFM-300(Sc) (black circles), MFM-300(Sc) in presence of 10% RH (red circles) and MFM-300(Sc) in presence of 20% RH (blue circles). All data are reported at 298 K.

Simulated Distributions of the SO_2 molecules within the pores

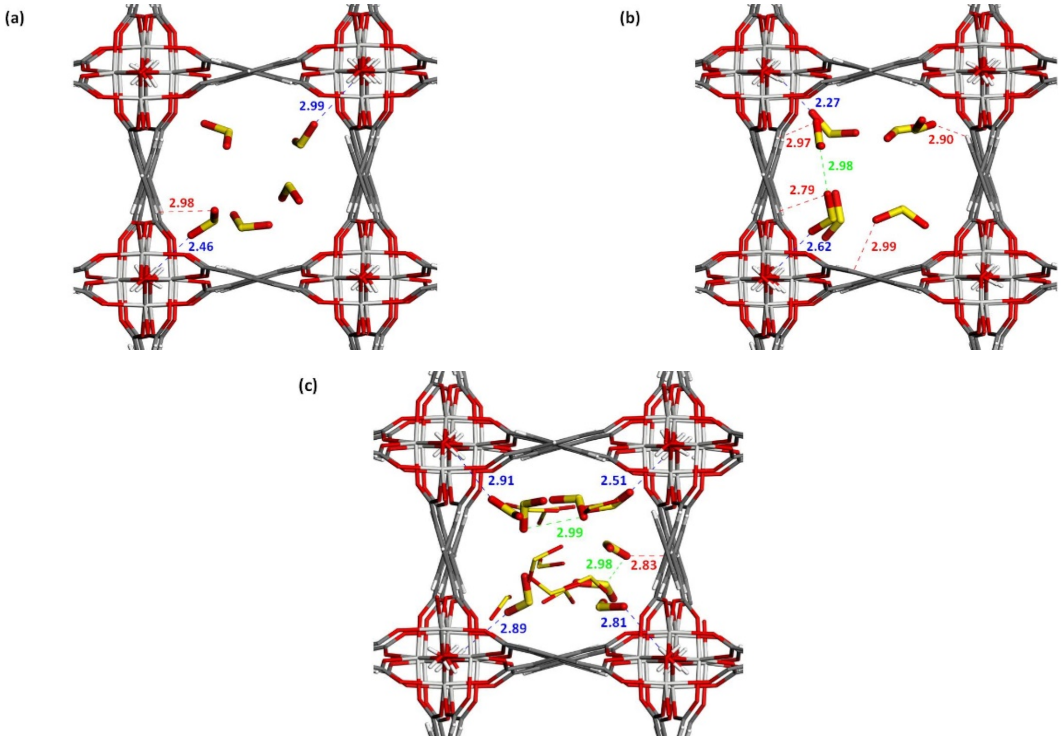

Fig. S15. Snapshots extracted from MC simulations for different loadings of SO_2 as single components (a) 12.5 molecules of SO_2 per unit cell (b) 25 molecules of SO_2 per unit cell (c) 50 molecules of SO_2 per unit cell. The distances are reported in Å. (Sc, light gray; O, red; S, yellow; C, grey; H, white). (Interaction (Dashes lines): O_{So2}-$H_{\mu\text{-}OH}$(Blue), O_{SO2}-C_{org}(Red), S_{SO2}-O_{SO2}(Green), S_{SO2}-O_{SO2}(Green)).

Simulated Distributions of the SO_2/CO_2 molecules within the pores

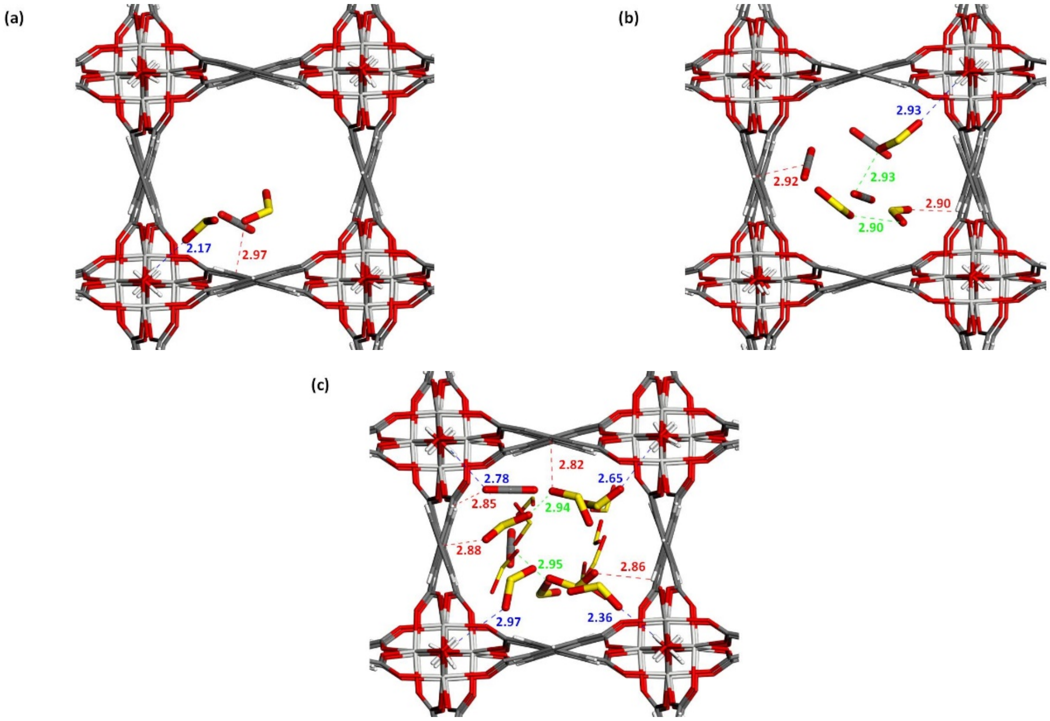

Fig. S16. Snapshots extracted from MC simulations for different loads of SO_2/CO_2: (a) 5 molecules of SO_2 and 1 molecule of CO_2 per unit cell (b) 15 molecules of SO_2 and 3.5 molecules of CO_2 per unit cell (c) 42.5 molecules of SO_2 and 5.25 molecules of CO_2 per unit cell. The distances are reported in Å. (Sc, light gray; O, red; S, yellow; C, grey; H, white). (Interaction (Dashes lines): O_{So2}-$H_{\mu\text{-OH}}$(Blue), O_{So2}-$H_{\mu\text{-OH}}$ (Blue), O_{SO2}-C_{org}(red), O_{CO2}-C_{org}(red), S_{SO2}-C_{org}(red), C_{CO2}-C_{org}(red), S_{SO2}-O_{SO2}(Green), O_{SO2}-O_{SO2}(Green), O_{CO2}-O_{CO2}(Green), C_{CO2}-O_{CO2}(Green), O_{SO2}-O_{CO2}(Green), S_{SO2}-C_{CO2}(Green)).

Radial Distribution Functions

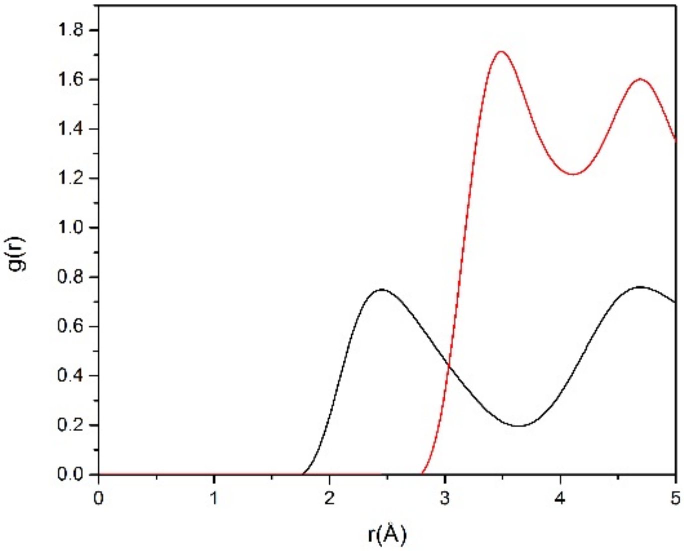

Fig. S17. Radial distribution functions calculated in the case of the adsorption of SO_2 as single component for the SO_2/MOF pairs: $H_{\mu\text{-OH}}$-O_{SO2}(Black), C_{org}–O_{SO2}(Red) (50 molecules of SO_2 per unit cell).

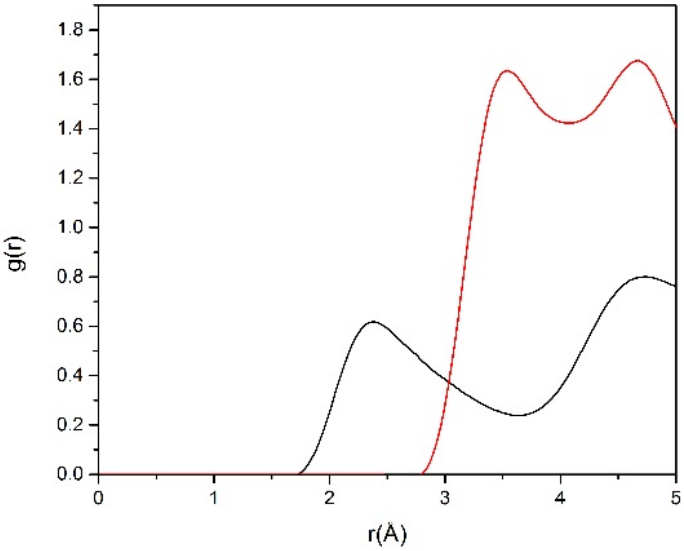

Fig. S18. Radial distribution functions calculated in the case of the adsorption of CO_2 as single component for the CO_2/MOF pairs: $H_{\mu\text{-OH}}$-O_{CO2}(Black), C_{org}–O_{CO2}(Red) (31.5 molecules of CO_2 per unit cell).

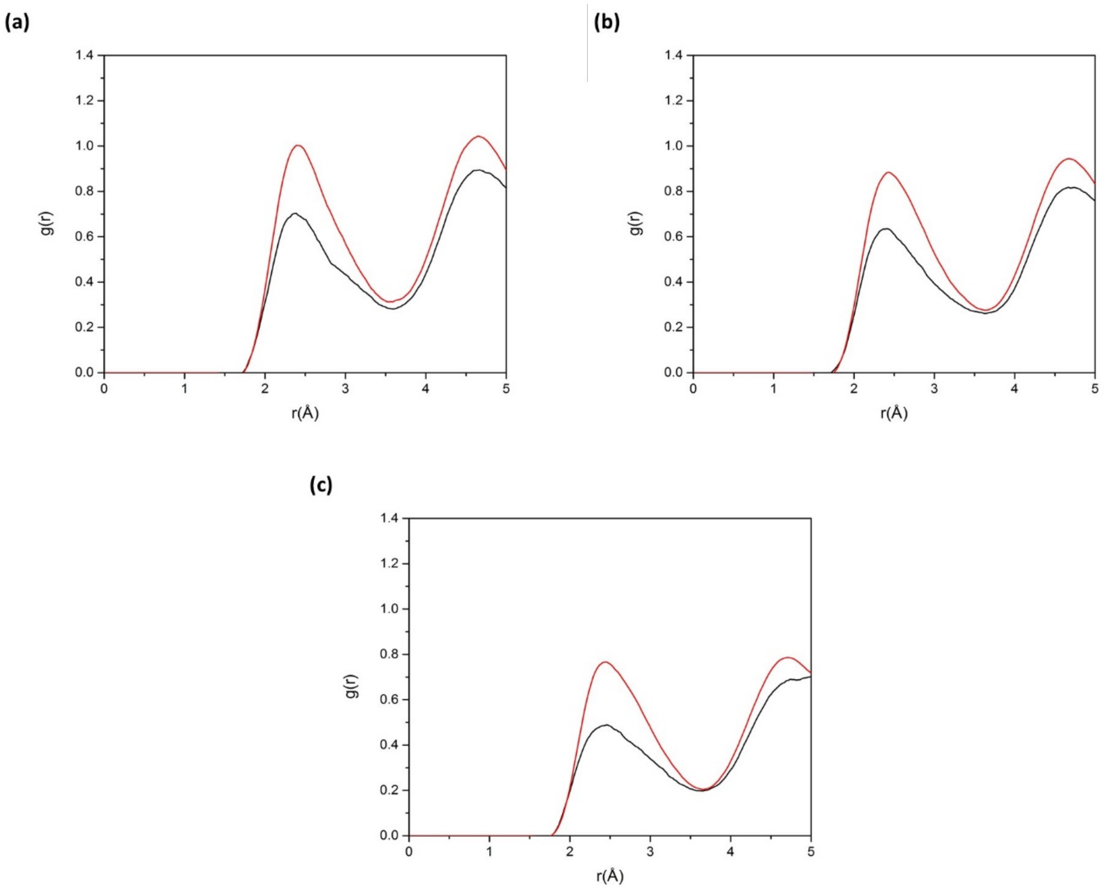

Fig. S19. Radial distribution functions calculated in the case of the co-adsorption of SO_2/CO_2 (binary mixture molar gas composition: 20:80) component for the CO_2/MOF and SO_2/MOF pairs: (a) $H_{\mu\text{-}OH}$-O_{SO2}(Red), $H_{\mu\text{-}OH}$-O_{CO2}(Black) (5 molecules of SO_2 and 1 molecule of CO_2 per unit cell), (b) $H_{\mu\text{-}OH}$-O_{SO2}(Red), $H_{\mu\text{-}OH}$-O_{CO2}(Black) (15 molecules of SO_2 and 3.5 molecules of CO_2 per unit cell), (c) $H_{\mu\text{-}OH}$-O_{SO2}(Red), $H_{\mu\text{-}OH}$-O_{CO2}(Black) (42.5 molecules of SO_2 and 5.25 molecules of CO_2 per unit cell).

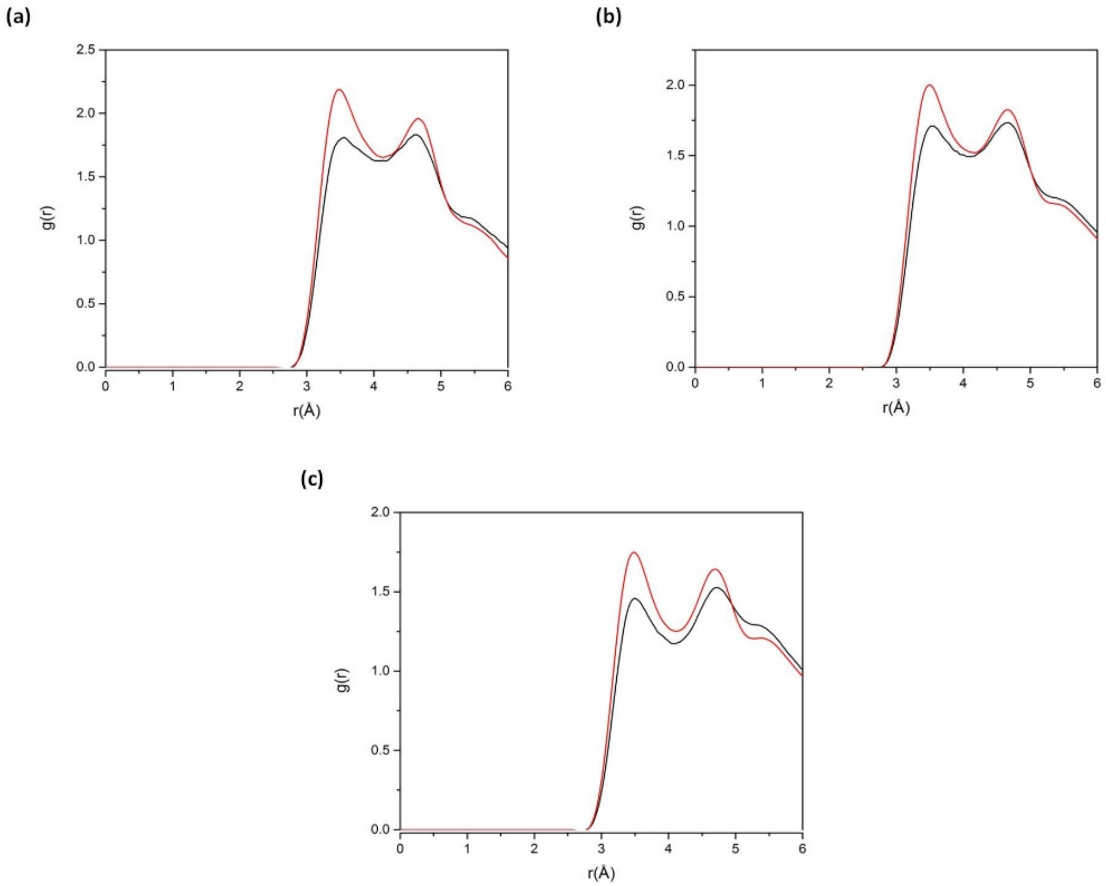

Fig. S20. Radial distribution functions calculated in the case of the co-adsorption of SO_2/CO_2 (binary mixture molar gas composition: 20:80) component for the CO_2/MOF and SO_2/MOF pairs: (a) C_{org}-O_{SO2}(Red), C_{org}-O_{CO2}(Black) (5 molecules of SO_2 and 1 molecule of CO_2 per unit cell), (b) C_{org}-O_{SO2}(Red), C_{org}-O_{CO2}(Black) (15 molecules of SO_2 and 3.5 molecules of CO_2 per unit cell), (c) C_{org}-O_{SO2}(Red), C_{org}-O_{CO2}(Black) (42.5 molecules of SO_2 and 5.25 molecules of CO_2 per unit cell).

Calculation of the accessible surface area and free pore volume of MFM-300(Sc).

The calculation of the accessible surface area (Sacc) is based on the geometric topology of the adsorbent and performed using a simple Monte Carlo integration technique where the centre of mass of the probe molecule with hard sphere is “rolled” over the framework surface. In this method, a nitrogen-sized (3.6Å) probe molecule is randomly inserted around each framework atom of the adsorbent and the fraction of the probe molecules without overlapping with the other framework atoms is then used to calculate the accessible surface area. The LJ size parameters of the framework atoms were those considered using the UFF[12] force field. The free pore volume was calculated considering a probe molecule of 0 Å.

10. Synthesis of MFM-300(Al) and SO_2 experiments

Synthesis of MFM-300(Al): This MOF material it was synthesised according to a previous reported methodology,[23] with a slight modification: H_4L^1= biphenyl-3,3'5,5'-tetracarboxylic acid (0.06 g, 0.182 mmol), $Al(NO_3)_3{\cdot}9H2O$ (0.34 g, 0.906) and piperazine (0.10 g, 1.26 mmol) were mixed and dispersed in water (10.0 ml), and HNO_3 (2.8 M, 2.0 mL) was subsequently added to the resulting slurry solution. The slurry solution was transferred into Teflon autoclave, which was sealed and heated up to 483 K for 72 h. After cooling over 12 h to room temperature, the resulting white microcrystalline product was separated by hand from the amorphous powder, filtrated, washed with water and dried in air. Yield: 0.025 g (20%). For SO_2 sorption experiments it was used a total of 0.0075g form 5 different reaction batches, combined them and then corroborated the purity of the material by PXRD (see Fig.S21).

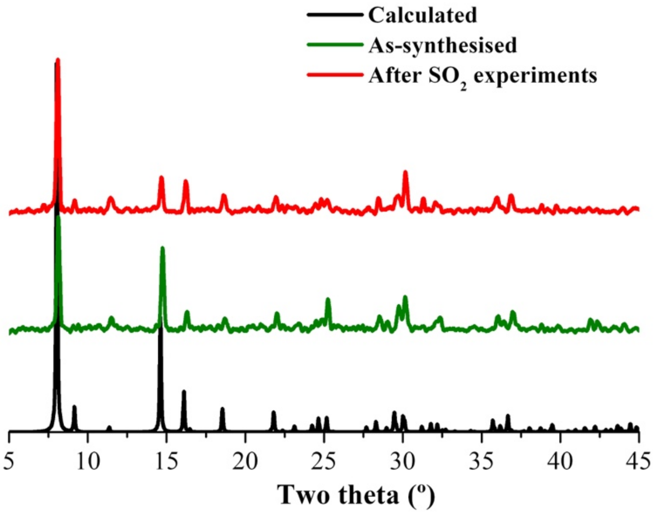

Fig. S21. Simulated (calculated) PXRD pattern for MFM-300(Al), (black), the as-synthesised (experimental) pattern (green) and for the pattern of MFM-300(Al) after the SO_2 adsorption (red).

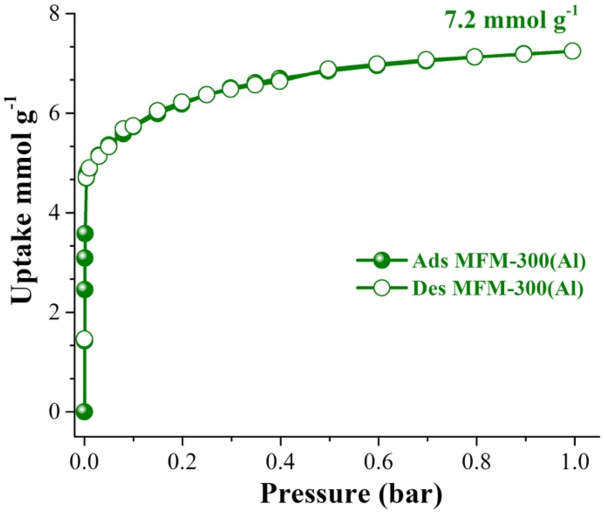

Fig. S22. SO_2 adsorption isotherm of MFM-300(Al) at 298 K and 1 bar.

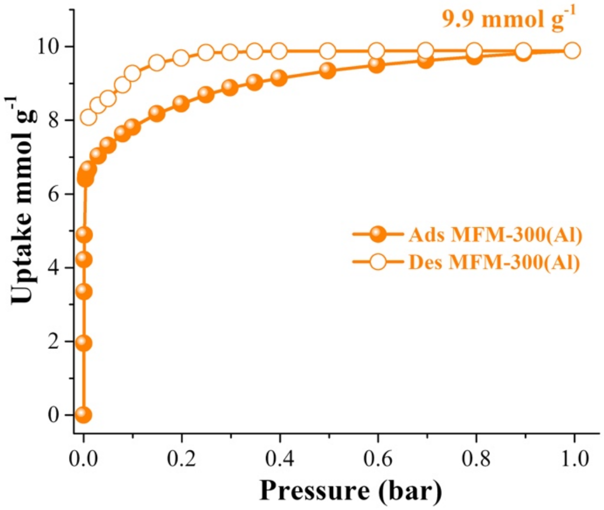

Fig. S23. SO_2 adsorption isotherm of EtOH@MFM-300(Al) at 298 K and 1 bar.

11. SO_2 cycling experiments for MFM-300(Sc)

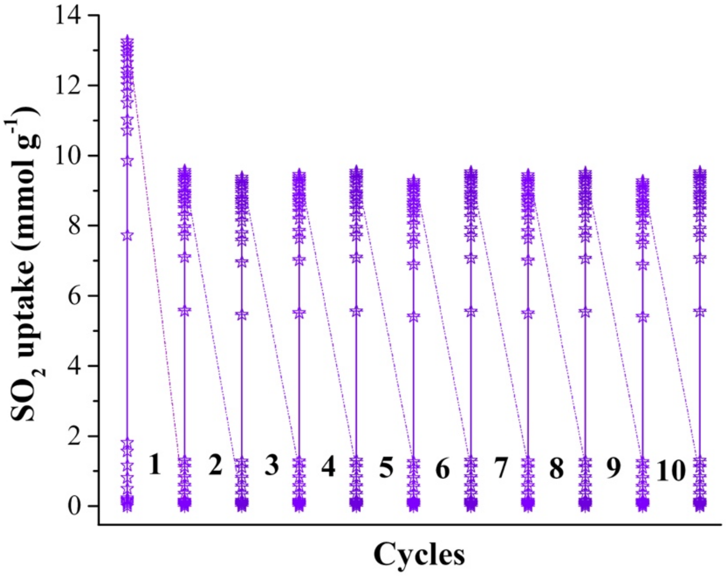

Fig. S24. Adsorption-desorption cycles for SO_2 in EtOh@MFM-300(Sc) at 1 bar and 298 K. The re-activation of this sample was conducted by only applying vacuum (1.7×10-6 Torr) for 30 minutes at room temperature (298 K).

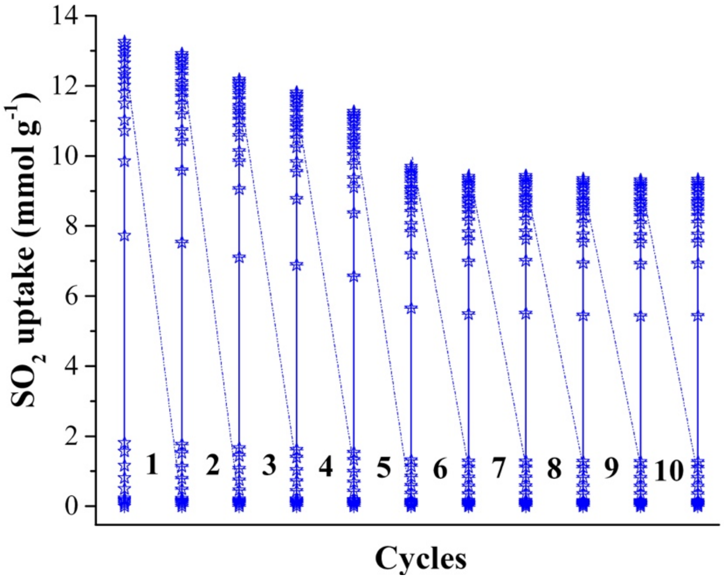

Fig. S25. Adsorption-desorption cycles for SO_2 in EtOh@MFM-300(Sc) at 1 bar and 298 K, without the re-activation step.

References

1. I. A. Ibarra, S. Yang, X. Lin, A. J. Blake, P. J. Rizkallah, H. Nowell, D. R. Allan, N. R. Champness, P. Hubberstey and M. Schröder, *Chem. Commun.*, 2011, **47**, 8304.

2. Rouquerol, F.; Rouquerol, J.; Sing, K. S. W.; Llewellyn, P.; Maurin, G. Adsorption by Powders and Porous Solids: Priciples, Methodology and Applications, 2nd ed.; Academic Press: Oxford, UK, 2014.

3. CRC Handbook of Chemistry and Physics, 85th ed.; Lide, D. R., Ed.; CRC Press: Boca Raton FL, 2004.

4. A. L. Myers and J. M. Prausnitz, *AIChE J.*, 1965, **11**, 121.

5. C. M. Simon, B. Smit and M. Haranczyk, *Comput. Phys. Commun.*, 2016, **200**, 364.

6. B. P. Bering and V. V. Serpinskii. "Adsorption of mixtures of gases. I. Adsorption of ethylene and carbon dioxide on active carbon". In: Zhurnal Fizicheskoi Khimii 26 (1952), pp. 253.

7. M. Savage, Y. Cheng, T. L. Easun, J. E. Eyley, S. P. Argent, M. R. Warren, W. Lewis, C. Murray, C. C. Tang, M. D. Frogley, G. Cinque, J. Sun, S. Rudic, R. T. Murden, M. J. Benham, A. N. Fitch, A. J. Blake, A. J. Ramirez-Cuesta, S. Yang, and M. Schröder, *Adv. Mater.*, 2016, **28**, 8705.

8. Rolando M.A. Roque-Malherbe. Adsorption and Diffusion in Nanoporous Materials. Boca Raton: CRC Press, 2007.

9. I. A. Ibarra, A. Mace, S. Yang, J. Sun, S. Lee, J.-S. Chang, A. Laaksonen, M. Schröder and X. Zou, *Inorg. Chem.*, 2016, **55**, 7219.

10. Shaheen A. Al-Muhtaseb and James A. Ritter. "Roles of Surface Heterogeneity and Lateral Interactions on the Isosteric Heat of Adsorption and Adsorbed Phase Heat Capacity". In: The Journal of Physical Chemistry B 103.13 (1999), pp. 2467.

11. S. L. Mayo, B. D. Olafson and W. A. Goddard, *J. Phys. Chem.,* 1990, **94**, 8897.

12. A. K. Rappe, C. J. Casewit, K. S. Colwell, W. A. Goddard and W. M. Skiff, *J. Am. Chem. Soc.,* 1992, **114**, 10024.

13. S. Hamad, S. R.G. Balestra, R. Bueno-Perez, S. Calero, A. R. Ruiz-Salvador, *Journal of Solid State Chemistry*, 2015, **223**, 144.

14. J. P. Perdew, K. Burke and M. Ernzerhof, *Phys. Rev. Lett.*, 1996, **77**, 3865.

15. W. J. Hehre, J. A. Ditchfeld and J. A. Pople, *J. Chem. Phys.*,1972, **56**, 2257.

16. M. B. H. Ketko, G. Kamath, and J. Potoff, *J. Phys. Chem. B*, 2011, **115**, 4949.

17. J. Potoff, and J.I. Siepmann, *AIChE J.*, 2001, **47**, 1676.

18. J. L. F. Abascal and C. Vega, *J. Chem. Phys.*, 2005,**123**, 234505.

19. (a) E. Sanchez-Gonzalez, P. G. M. Mileo, J. R. Alvarez, E. Gonzalez-Zamora, G. Maurin and I. A. Ibarra, *Dalton Trans.,* 2017, **46**, 15208; (b) D. D. Borges, P. Normand, A. Permiakova, R. Babarao, N. Heymans, D. S. Galvao, C. Serre, G. De Weireld and G. Maurin, *J. Phys. Chem. C,* 2017, **121**, 26822. (c) E. Sánchez-González, P. G. M. Mileo, M. Sagastuy-Breña, J. R. Álvarez, J. E. Reynolds, A. Villarreal, A. Gutiérrez-Alejandre, J. Ramírez, J. Balmaseda, E. González-Zamora, G. Maurin, S. M. Humphrey and I. A. Ibarra, *J. Mater. Chem. A*, 2018, **6**, 16900.

20. O. N. Osychenko, G. E. Astrakharchik and J. Boronat, *Mol. Phys*., 2012, **110**, 227; (b) J. Kolafa and J. W. Perram*, Mol. Simul*., 1992, **9**, 351.

21. Q. Yang, D. Liu, C. Zhong and Jian-Rong Li, *Chem. Rev*. 2013, **113**, 826.

22. T. J. H. Vlugt, E. Garcıa-Perez, D. Dubbeldam, S. Ban and S. Calero, *J. Chem. Theory Comput.*, 2008, **4**, 1107.

23. S. Yang, J. Sun, A. J. Ramirez-Cuesta, S. K. Callear, W. I. F. David, D. P. Anderson, R. Newby, A. J. Blake, J. E. Parker, C. C. Tang and Martin Schröder, *Nature Chemistry*, 2012, **4**, 887.